Available online at www.sciencedirect.com

SCIENCE DIRECT®

Journal of Marine Systems 56 (2005) 45–66

JOURNAL OF MARINE SYSTEMS

www.elsevier.com/locate/jmarsys

A rapid response nowcast/forecast system using multiply nested ocean models and distributed data systems

Reiner Onken[a,*,1], Allan R. Robinson[b], Lakshmi Kantha[c], Carlos J. Lozano[b], Patrick J. Haley[b], Sandro Carniel[d]

[a]GKSS Research Center, Institute for Coastal Research, Max-Planck-Str. 1, 21502 Geesthacht, Germany
[b]Harvard University, Cambridge, MA, USA
[c]University of Colorado, Boulder, CO, USA
[d]CNR-ISMAR, Institute of Marine Sciences, Venice Section, San Polo 1365, I-30125 Venice, Italy

Received 15 July 2003; accepted 6 September 2004
Available online 9 December 2004

Abstract

Logistics and results of a real-time modeling effort, which took place in fall 2000 in the waters between Corsica and Italy in the Mediterranean Sea, are presented. The major objective was to nest a high-resolution local version of the Harvard Ocean Prediction System (HOPS) into a coarse resolution Colorado University Princeton Ocean Model (CUPOM) covering the northern part of the Western Mediterranean. Due to the different designs of CUPOM and HOPS, traditional nesting methods were not successful. Therefore, a new method was developed that assimilated the CUPOM prognostic fields into HOPS instead of prescribing them only along the open boundaries. Another objective of the effort was to set up and test a data distribution system, providing Internet-based rapid data transfer among the project partners being partly at sea and partly on land in different continents. It is shown that such a system works, enabling turnaround times of less than a day from the time when measurements are taken to the release of the model forecast.

Keywords: Ocean forecasting; Operational oceanography; Real-time modeling; Nesting; Distributed systems

1. Introduction

Operational ocean forecast models are now available on all scales from global (e.g. US Naval Research Laboratory Eddy Resolving Model) to local (e.g. US Naval Oceanographic Office Shallow Water Analysis and Forecast System). Usually, such models are initialized by climatological fields when needed or, if direct measurements of oceanic parameters are

* Corresponding author. Tel.: +49 4152 87 1546; fax: +49 4152 87 1525.
E-mail address: onken@gkss.de (R. Onken).
[1] Previous affiliation: SACLANT Undersea Research Centre, La Spezia, Italy.

0924-7963/$ - see front matter © 2004 Elsevier B.V. All rights reserved.
doi:10.1016/j.jmarsys.2004.09.010

available for the region of interest, by melding climatology with observations. In only a few cases with sufficient coverage by direct measurements, the models may be initialized solely from observations (Onken et al., 2003). In order to make the forecasts as close as possible to reality, the models are driven by synoptic atmospheric forcing fields and by assimilation of real-time observations, which may consist of remotely sensed data and/or in situ measurements.

The formulation of the open boundary conditions is a fundamental problem arising for model domains on sub-global scale. There exist different methodologies for prescribing the flow and tracer fields along the boundaries (Orlanski, 1976; Spall and Robinson, 1990), the objective of which is to make them dynamically consistent and to prevent the interior fields from contamination by spurious boundary effects. The shortcoming of this method is that features and events outside the domain that might affect the interior dynamics are not represented. In order to take account of those, nesting of model domains is desirable. Nesting means that a fine resolution model is embedded in a coarse resolution domain, enabling communication between both across the joint boundaries, either in both directions (two-way nesting) or from coarse to fine only (one-way nesting). Both nesting and input from in situ data are viable approaches to running a local forecast model. However, the latter requires appropriate observational resources to be brought to bear upon the problem, which may be either expensive or often unfeasible.

For application to fisheries management and for naval operations, fine resolution ocean forecasts are frequently required for limited regions with open boundaries. In a few cases, there already exists a larger-scale, coarse resolution model, and it is highly desirable to nest a fine resolution model into the coarse model. In fall 2000, the participants of the joint research project Multi-Scale Environmental Assessment Network Studies (MEANS, 19 September–9 October) were faced with such a problem: for naval research, there was a demand for an operational ocean forecast of the waters around the island of Elba in the Mediterranean Sea (see Fig. 1). As the required resolution was O(1 km) on the larger scale but O(100 m) along the Elba shoreline, a nested configuration was selected. For computational efficiency reasons, the coarse resolution model domain (to be referred to as "C domain" or "C model") was designed to extend zonally from Corsica to the Italian mainland ($\approx$130 km) and 80 km meridionally, having open boundaries in the north and in the south, while the dimensions of the high-resolution nest ("D domain") were about 40×40 km encompassing Elba. In order to improve the forecast quality of the C domain, there was a need to nest the C domain into an existing coarse resolution operational model covering the entire Mediterranean (the "A domain"). As the resolution of the A domain was much lower than that of the C domain, another nest (the "B domain") was introduced at an intermediate resolution covering the Ligurian Sea.

If both the coarse and the fine resolution model are of the same type and technically identical, and if their horizontal and vertical grids are collocated, then the nesting procedure is straightforward: by interpolation of the prognostic variables between the grids. However, if the models are different (i.e. equations, finite difference schemes, bathymetry, assimilation schemes, and forcing fields are not identical, grids non-collocating), the conventional nesting method fails. In the present case, the Colorado University Princeton Ocean Model CUPOM is applied to the B domain, whereas for the C and D domains the Harvard Ocean Prediction System HOPS is used. Naval Oceanographic Office (NAVOCEANO, Stennis Space Center, MS, USA) operational Shallow Water Analysis and Forecast System (SWAFS, Horton et al., 1997) exists for the A domain, and it is based on CUPOM. Hence, both the nesting of B into A and D into C did not cause any major trouble, but the nesting between the B and C domains was delicate. Therefore, we will concentrate on the latter. For results of the A→B one-way nesting and the C→D two-way nesting modeling efforts, the reader is referred to Carniel et al. (2001), Kantha et al. (2002) and Robinson et al. (submitted for publication).

MEANS was conducted within the framework of Rapid Environmental Assessment (REA), which is a long-term research program of the North Atlantic Treaty Organization NATO. Concerning ocean modeling, "rapid" means that forecasts of the state of the

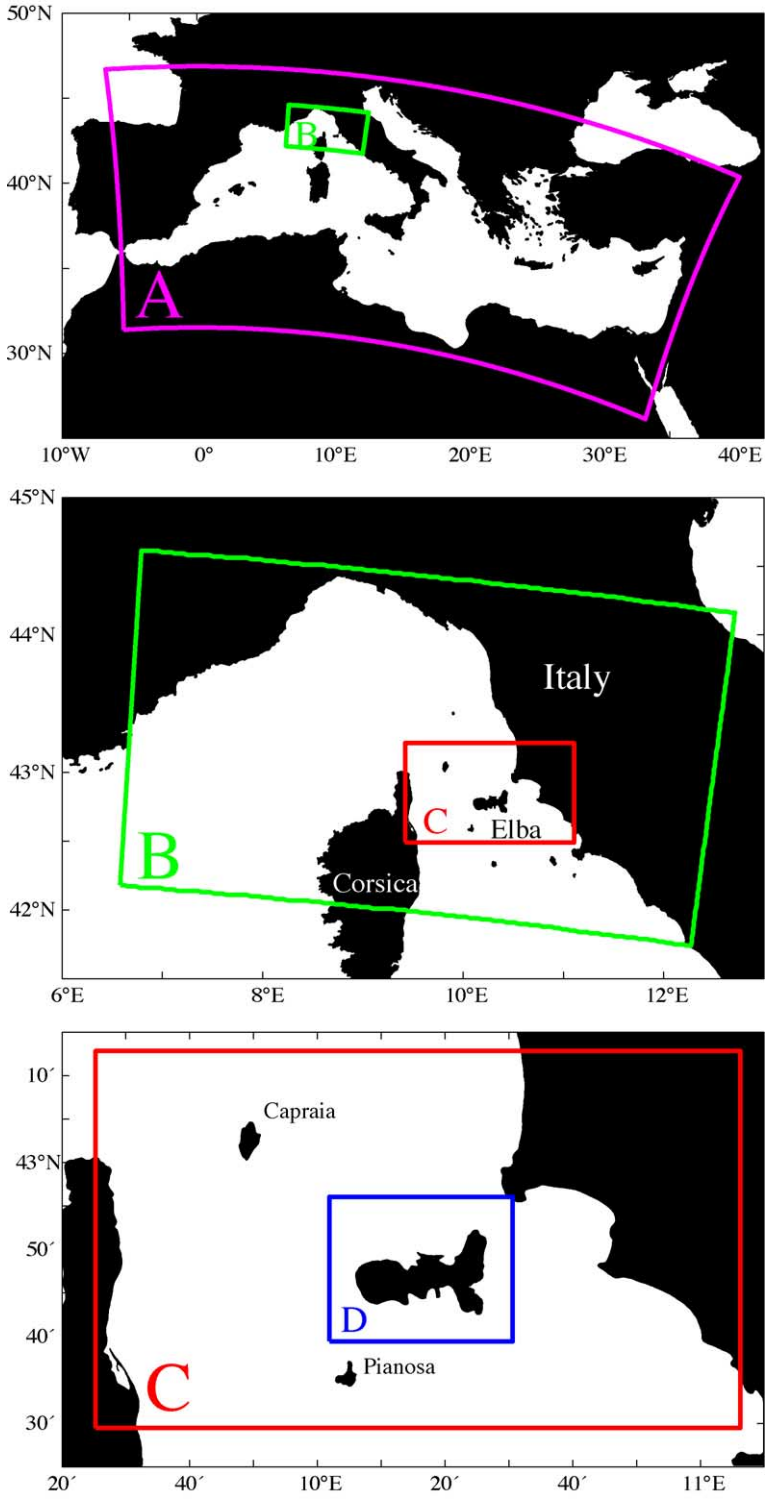

Fig. 1. Arrangement of model domains. Domains A and B are CUPOM, C and D are HOPS.

ocean have to be provided in real time on a daily basis, taking account of the most recent observations. This requires a streamlined procedure consisting of taking the measurements, processing the data, feeding the data into the forecast models, to run the model, process the results, and return the results to the customers. As the allowed time for this is about 1 day, it is necessary to set up a viable scheme for rapid data transmission.

The principal objective of this work is to show that high-resolution ocean forecast modelling can be provided for a limited exercise area, by using existing larger-scale forecast models for updating the open boundaries. As a secondary objective, we will demonstrate the complexity of the logistics coming along with such modeling effort within the scope of REA, i.e. to disseminate rapidly observational data and forecast results to all team members. In the following section, we will first present the real-time data used for model initialization and assimilation, the outline of the forecast experiment and the way various data were exchanged between the MEANS project participants. The models are described in Section 3 and the nesting method between the B and C domains in Section 4. In Section 5, we will compare first the forecasts of the B and the C model for the C domain, while the C domain is running in unnested mode, and then investigate the effects of the B→C nesting.

2. Experimental design

2.1. Real-time data

For accurate ocean prediction, real-time observations of temperature and salinity distributions are required in order to initialize forecast models from a situation which is as close as possible to reality, and also for intermittent updates of the model solution. During MEANS, these observations were conducted by the NATO Research Vessel *Alliance*. The initialization survey took place from 19 to 25 September, covering the waters between 42°30′N and 44°N and between 9°30′ and the Italian mainland with an almost equally spaced grid of 106 conductivity–temperature–depth (CTD) casts. The nominal distance between the casts was 7.5′ corresponding to 7.5 nautical miles south–north and about 5.5 miles west–east (Fig. 2). This is sufficient to resolve the Rossby radius which is around 15 km in this area for that time of the year. Daily update surveys, conducted from 24 September to 9 October and employing 76 CTD, 44 expendable CTD (XCTD), and 75 expendable bathythermograph (XBT) casts, were confined to the C domain. The update casts were confined to the waters around Elba focusing on the D domain, and to the region between Elba, Capraia and the Italian mainland to take a close look at the evolution of the Capraia eddy (cf. Robinson et al., submitted for publication). The positions were determined on short notice and guided by interpretation of the most recent forecast for the C and D domains, in other words through adaptive sampling.

2.2. Forecast plan

Out of the four models, the A model was the only operational one providing continuous updates of ocean parameters for the Mediterranean around the year. It is run daily by the United States Navy at the Naval Oceanographic Office (NAVOCEANO) and produces a nowcast and a 2-day forecast. The B model was run at the SACLANT Undersea Research Centre (SACLANTCEN, La Spezia, Italy), but in delayed mode of about 24 h, because it had to wait for boundary conditions extracted from the A model for the one-way nesting. In the same way, data subsets of the B model were provided as boundary conditions for the C model which was run at Harvard University (Cambridge, MA, USA). As the B→C nesting was considered to be experimental, C was run operationally every day in a safe standalone mode without nesting (referred to as C_{sa}) using open boundary conditions, and a nested experimental mode C_{nest}.

2.3. Data exchange

From precursor studies it had turned out that an operational system works most efficiently, if the project partners remain at their home location as far as possible, i.e. the HOPS team at Harvard and the CUPOM team partly at Colorado University and partly at SACLANTCEN because of the direct access

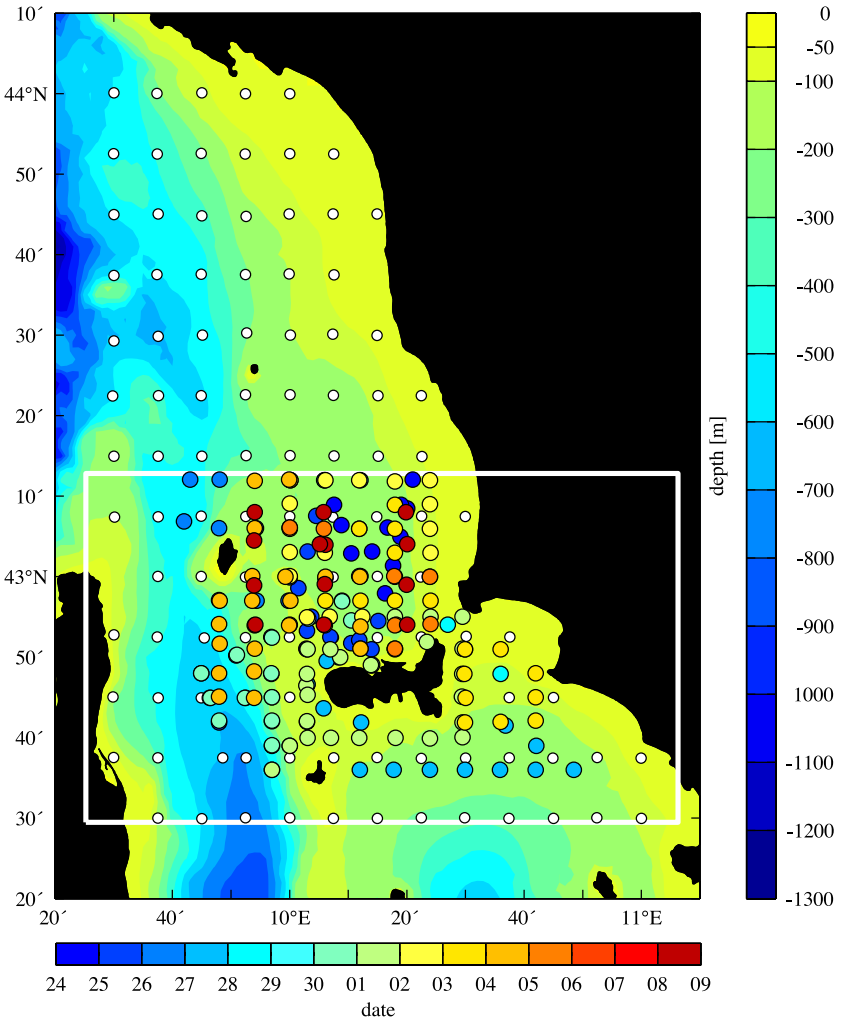

Fig. 2. Positions of casts during the initialization survey (19–23 September, white circles) and the update surveys (24 September–9 October, colored circles). During the initialization survey, only CTD casts were taken, while during the update also XBTs and XCTDs were used. The color of the circles of the update survey provides information on the time when the cast was taken. The color refers to the horizontal color bar representing the time period 24 September–9 October. The boundary of the C model domain is indicated by the white rectangle, water depth is represented by the background color and refers to the vertical color bar.

to the large volume SWAFS and COAMPS data sets. In consequence of that a sophisticated data distribution system was developed, enabling rapid exchange of data (Fig. 3) among the MEANS project partners at sea and on land in Europe and in the USA. The core of the system was the MEANS server, a World Wide Web server located at SACLANTCEN. Products of almost all participants were uploaded to the server making them accessible to everyone involved. NRV *Alliance* provided in situ observations for assimilation into the B model run at SACLANTCEN, and the C and D models run at Harvard University. Harvard University in turn uploaded graphical output of the C and D domains and updated survey plans for adaptive sampling by *Alliance* based on the model results. For the B model runs at SACLANTCEN, the A domain output was downloaded from NAVOCEANO, and Coupled Ocean Atmosphere Mesoscale Prediction System (COAMPS) atmospheric forcing fields from Fleet Numerical Meteor-

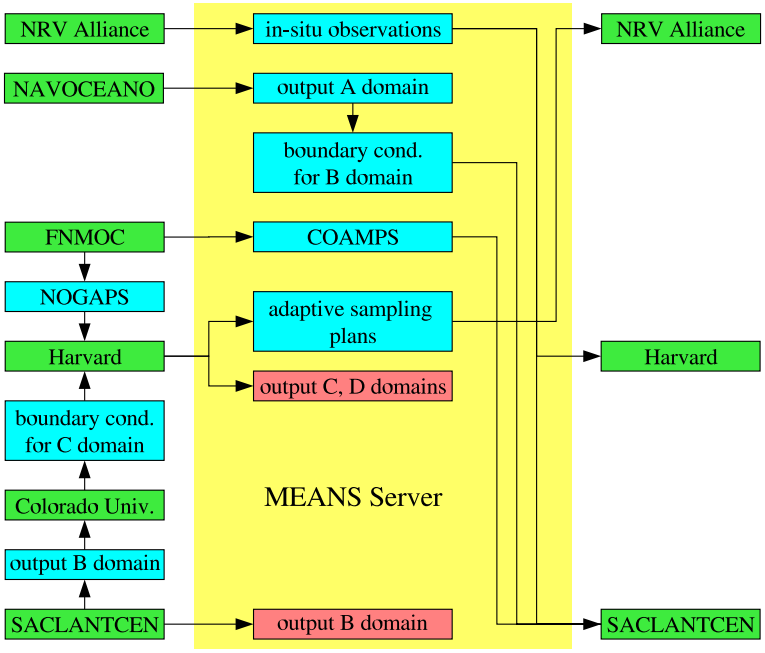

Fig. 3. Diagram illustrating the data exchange between project participants. Contributing institutions are colored green, graphics products pink and data blue. The yellow box is the MEANS server at SACLANTCEN. The diagram is cyclic in the left–right direction, i.e. NRV *Alliance*, Harvard University and SACLANTCEN are both uploading to and downloading from the server. Graphics products were accessible for all participants.

ology and Oceanography Center (FNMOC, Monterey, CA, USA), while the B model output was uploaded by SACLANTCEN. In order to minimize upload/download times, some data traffic occurred outside the MEANS server. This is the numerical output of the B model, which was sent from SACLANTCEN to Colorado University. There, boundary conditions for the C domain were extracted and then sent to Harvard University. Another short route existed between Harvard University and FNMOC for direct downloading of Navy Operational Global Atmospheric Prediction System (NOGAPS) atmospheric forcing.

Fig. 3 looks rather simple, because it does not contain a time coordinate. There were, however, conditions imposing temporal constraints on the schedule:

- The update surveys by NRV *Alliance* could be conducted at night only, because the vessel was busy with other tasks during daytime. As the daytime work required 12 h attendance of the entire deck's crew, there was no crew available between midnight and 08:00 next morning. Therefore, the surveys consisted of CTD casts between 20:00 and midnight, and XCTD/XBT cast after midnight which did not require support by the deck's crew.
- The upload of the A model output from NAVOCEANO and the COAMPS atmospheric forcing from FNMOC started routinely at 05:00 Central European Summer Time (CEST) by automatic File Transfer Protocol (FTP). Because of the large volumes of more than 200 Megabyte, this transfer lasted between 3 and 5 h.
- The B, C and D models were run on 500-MHz workstations (SUN Ultra10, DEC Alpha XP1000), which took several hours including a final quality control (despiking, plausibility check) of the survey data, preparation of assimilation fields, and output validation.
- As far as possible, working time had to be during daylight hours for the teams at Colorado and Harvard Universities and at SACLANTCEN.

Table 1
Schedule of activities during MEANS

CEST	Contributor	Activity	EDT/MDT	Contributor	Activity
20:00	*Alliance*	Start CTD survey	14:00	Harvard Univ.	Download boundary conditions for C_{nest} from Colorado
00:00	*Alliance*	Start XCTD/XBT survey	18:00	NAVOCEANO	Upload A model output
22:00			16:00	Harvard Univ.	Start C_{nest} run
03:00			21:00	Harvard Univ.	Upload C_{nest} forecast
07:00			01:00	FNMOC	Upload COAMPS forcing
11:00	*Alliance*	Upload night survey data	05:00		
11:30	SACLANTCEN	Download survey data	05:30	Harvard Univ.	Download survey data
12:00	SACLANTCEN	Download A model output, extract boundary conditions from A model output, download COAMPS forcing	06:00		
13:00	SACLANTCEN	Start B run	07:00	Harvard Univ.	Download NOGAPS forcing from FNMOC
14:00			08:00	Harvard Univ.	Start C_{nest} and D run
18:00	SACLANTCEN	Upload B model output	12:00		
18:30			10:30	Colorado Univ.	Download B model output
19:00			13:00	FNMOC	Upload COAMPS forcing
19:00			11:00	Colorado Univ.	Extract boundary conditions from B model output for C_{nest}
19:00			13:00	Harvard Univ.	Upload C_{nest} and D forecast, upload sampling plan
19:30	*Alliance*	Download sampling plan	13:30		

CEST: Central European Summer Time; EDT: Eastern Daylight Time; MDT: Mountain Daylight Time.

Keeping these constraints in mind, the project partners agreed on the schedule displayed in Table 1.

3. The models

3.1. CUPOM

CUPOM is based on the primitive equations Princeton Ocean Model (Blumberg and Mellor, 1987). It includes free-surface dynamics and in addition an improved turbulence closure model (Kantha and Clayson, 1994) based on the scheme developed originally by Mellor and Yamada (1982). The prognostic variables are arranged on an Arakawa C grid, and terrain-following sigma-coordinates are employed in the vertical direction. CUPOM has been applied to a variety of oceanic regions, in a hindcast and a nowcast/forecast mode. Examples include Lopez and Kantha (2000), Carniel et al. (2002), Bang et al. (1996), and Kantha et al. (1999).

For the A domain, the SWAFS model running in operational mode at NAVOCEANO is similar to CUPOM. The horizontal resolution is 10 km, and 19 sigma levels are used in the vertical. The model is driven by surface fluxes derived from six hourly COAMPS fields at 0.2° horizontal resolution. Sea surface height (SSH) from satellite altimeter data and remotely sensed sea surface temperature (SST) are assimilated routinely using a simple Optimum Interpolation based nudging scheme.

In the B domain, CUPOM is initialized with SWAFS temperature and salinity fields and with the CTD data of the initialization survey. The horizontal resolution is 3 1/3 km, the vertical discretization and the atmospheric forcing is the same as in the A domain. Survey data from *Alliance* and SST were assimilated whenever available. SSH was not assimilated because of non-availability in real-time at SACLANTCEN where the B domain was run. Topography was derived from NAVOCEANO DBDB-V database.

For the A→B nesting, the B model is driven by boundary conditions from the A model along the two open boundaries in the west and in the south. The values along the boundaries in terms of SSH,

horizontal velocity, temperature and salinity are given by interpolation of the A model values, saved every 40 min (B model time step 2 min).

For every day N, the B model was initialized at day $N-1$ from the previous days nowcast and integrated for 72 h. Output was dumped in half-day intervals at times $N-0.5$, N (the "nowcast"), $N+0.5$, $N+1$ (1-day forecast), $N+1.5$ and $N+2$ (2-day forecast), which was used for visualization of model results and also for providing boundary conditions to the C domain.

3.2. HOPS

Detailed descriptions of HOPS can be found in Robinson (1996, 1999), Robinson et al. (1996) and Lozano et al. (1996). The heart of HOPS is a rigid-lid primitive equation model. The prognostic variables are arranged on an Arakawa B grid, and sigma-coordinates are employed in vertical direction. Horizontal subgridscale processes are parameterized by a Shapiro filter (Shapiro, 1970; Robinson and Walstad, 1987), vertical diffusion is formulated in terms of a Richardson number dependent scheme similar to that of Pacanowski and Philander (1981). Near horizontal and vertical rigid boundaries, Rayleigh friction is applied using a Gaussian weighting of distance from the bottom or the coast, respectively (Lermusiaux, 1997). The mixed layer physics is formulated according to Niiler and Kraus (1977).

For the C and D domains, 16 sigma levels are used in the vertical, which is sufficient to resolve the water masses. The bathymetry is DBDB-V (obtainable from NAVOCEANO, via Internet address http://www.navo.navy.mil/) at 1′ horizontal resolution, and the horizontal resolution is 675 and 225 m, respectively. Atmospheric forcing is provided by FNMOC by means of NOGAPS forcing fields at 1° horizontal resolution. Both domains are initialized from CTD data of the initialization survey. During the course of the integration, Optimum Interpolation (Carter and Robinson, 1987; Robinson et al., 1998) is used to generate assimilation fields of temperature and salinity from the initialization and update surveys in 1-day intervals, employing a spatial correlation scale of 15 km and a temporal correlation scale of 2 days. These fields are assimilated every 3 h, with linearly increasing assimilation weight towards their nominal time ("ramping").

For the C_{sa} model run (no B→C nesting), Orlanski (1976) radiation conditions are applied to the open boundaries for tracers, velocity and stream-function, while conditions according to Spall and Robinson (1990) are used for vorticity. With respect to the initialization and the assimilation of survey data, the C_{nest} runs were identical to C_{sa}, but in addition to using open boundary conditions, they were forced by the B domain fields. The method is explained below.

4. Nesting HOPS into CUPOM

For one-way communication between the B domain and the C domain, an attempt was made to prescribe the B domain tracer and velocity fields along the open boundary of the C domain applying conventional nesting techniques, i.e. interpolating the large domain prognostic variables on the open boundaries of the nest. However, we failed to formulate a scheme conserving mass, heat and salt, mainly due to the different orientations of the horizontal grids (the CUPOM grid is rotated, while that of HOPS is not) and the different arrangement of layers in the vertical. Additionally, because CUPOM is free-surface and HOPS is rigid-lid, the specifications of the barotropic velocity along the boundaries caused severe problems.

Alternatively, the B model dumps of temperature T, salinity S, and the rotational parts of the internal mode velocity, u_{rot}, v_{rot} (which are by definition divergence-free), were assimilated into the C domain instead of defining them only along the open boundaries. In detail, the prognostic variables were linearly interpolated from the B grid onto the C grid, over the entire C grid. The interpolated fields are then assimilated in the near boundary region of the C grid, the assimilation being defined strongest along the C domain boundaries and then rapidly decaying towards the interior. To accomplish that, an error matrix is defined containing values between 0 and 1. A value of 0 means that the C domain field is completely replaced by the B domain field, while 1 means that the B domain fields are ignored. The matrix is set up in a way that the error is 0 along the boundaries and then linearly increases to 1 within the next eight grid intervals normal to the boundaries. Hence, the B model fields affect the C

solution only close to the open boundaries directly within a stripe of 5400 m, while it is not used elsewhere. The half-width of the stripe being about one order of magnitude smaller than the Rossby radius guarantees a free evolution of dynamical features in the C domain. This is reasonable, because it is believed that the C_{sa} results in the interior are more reliable than those of the B model due to higher resolution and a more sophisticated assimilation scheme. This technique guarantees more "numerical continuity" than just imposing CUPOM boundary conditions, by spreading the transition between CUPOM and HOPS over eight grid points instead to define the transition from HOPS dynamics to CUPOM dynamics between adjacent grid nodes. In addition, using both "boundary assimilation" and radiation-type boundary conditions allow small-scale noise to propagate out of the C domain.

5. Results

We will compare now the results of model runs B, C_{sa}, and C_{nest} for the geographical area covered by the C domain and for the period of time October 3–6. The B run was initialized on 3 October 00:00 from the nowcast issued 24 h earlier and integrated forward for 72 h. The corresponding C_{sa} and C_{nest} runs were initialized one day earlier on 2 October 00:00 from survey data and run for 5 days (Fig. 4). For the nested run, B domain data were extracted in 12-h intervals and assimilated into C, starting on 3 October 12:00. As the major intention of this paper is to investigate the impact of the B→C nesting technique, we will restrict ourselves in the following to the description and interpretation of temperature and horizontal velocity at the surface and at 30-m depth. More details on the performance of the B domain model can be found in Carniel et al. (2001) and Kantha et al. (2002).

5.1. The B domain

For the B domain at the surface and at 30-m depth (Figs. 5 and 6, top panels), the large-scale flow pattern south of Elba is cyclonic while it is anticyclonic north of the island during the whole time between October 3 and 6. The cyclonic flow is fed by northwestward currents along the Italian coast originating from the Tyrrhenian Sea. South of Elba, the flow attains a zonal orientation to the west, and when impinging on the Corsican coast, it splits in two branches: the major one is returning south to the Tyrrhenian and the other is heading north along Corsica. The southern branch is apparently part of the basin scale cyclonic circulation of the northern Tyrrhenian, which is a well-known permanent feature (cf. Krivosheya and Ovchinnikov, 1973; Krivosheya, 1983; Artale et al., 1994; Astraldi and Gasparini, 1994). North of Elba, an anticyclonic gyre of about 40 km in diameter is confined to the area between the islands of Elba and Capraia and the Italian mainland. Sometimes (Fig. 5b) this vortex exhibits a closed circulation, at other times it is open to the north (Fig. 5a). The anticyclone is fed by southward flow along the Italian coast and from the waters east of Elba by means of a strong current through the Piombino Channel, which is the gap between Elba and the mainland. In a companion paper (Robinson et al., submitted for publication) based on the same data set, this anticyclonic feature (the "Capraia Eddy") was clearly verified from direct current measurements and satellite infrared images. Another pattern worth mentioning is the permanent northwestward flow between Capraia and Corsica. It appears to be driven mainly by the Capraia Eddy outflow and by the northward Corsica coastal current.

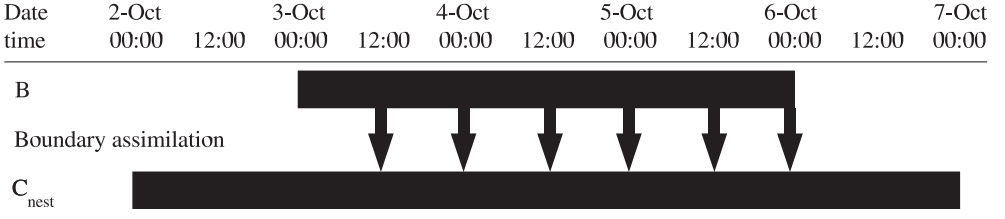

Fig. 4. Coupling of model runs discussed in this paper. The black bars represent the integration time of the B model and the C_{nest} runs; down arrows indicate updating of C_{nest} boundaries by B model output.

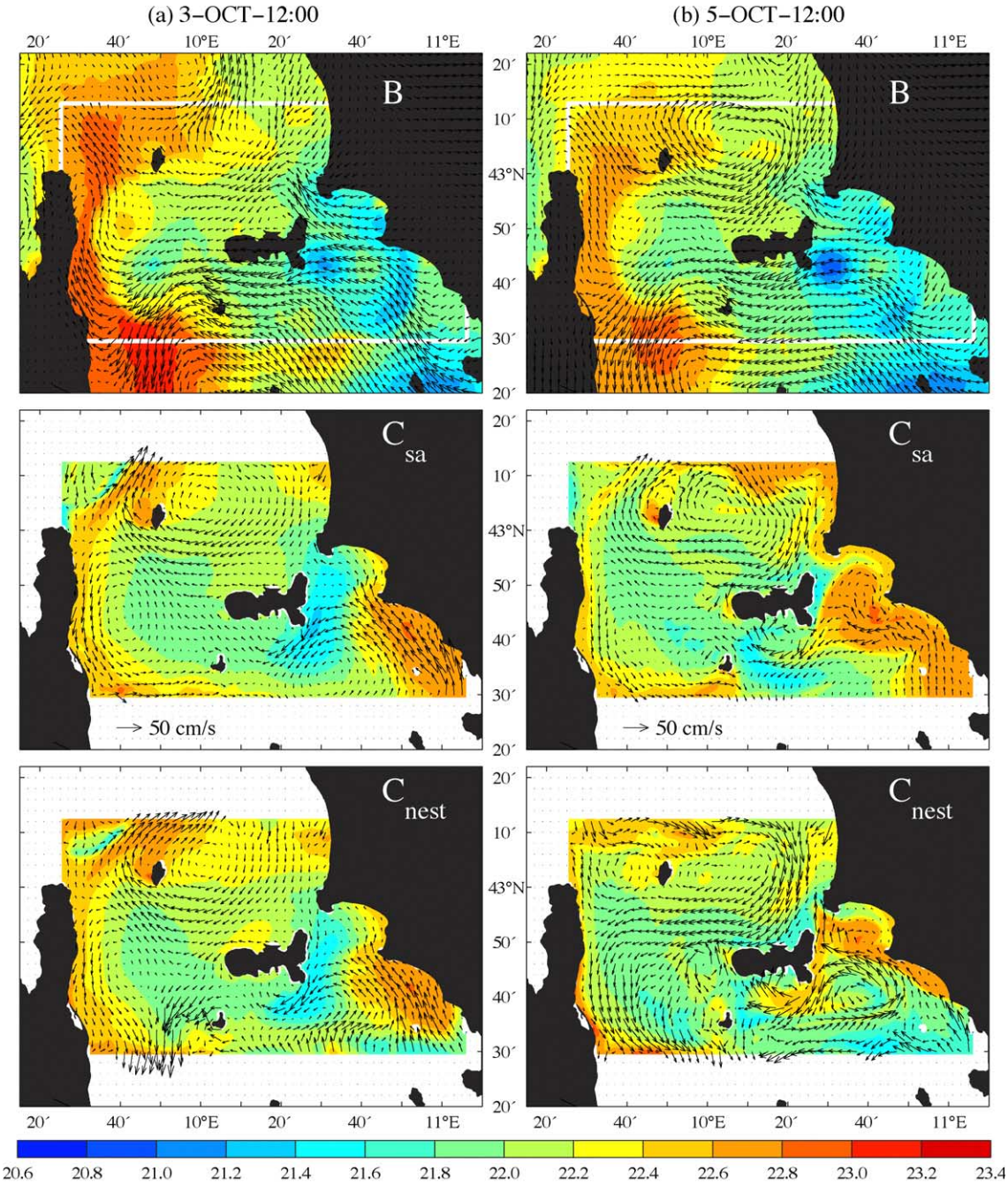

Fig. 5. Snapshots of surface velocity and temperature of model runs B (top), C_{sa} (center), and C_{nest} (bottom) (a) at the beginning and (b) towards the end of the nested configuration. The velocity scale is the same for all panels and indicated in the center panel.

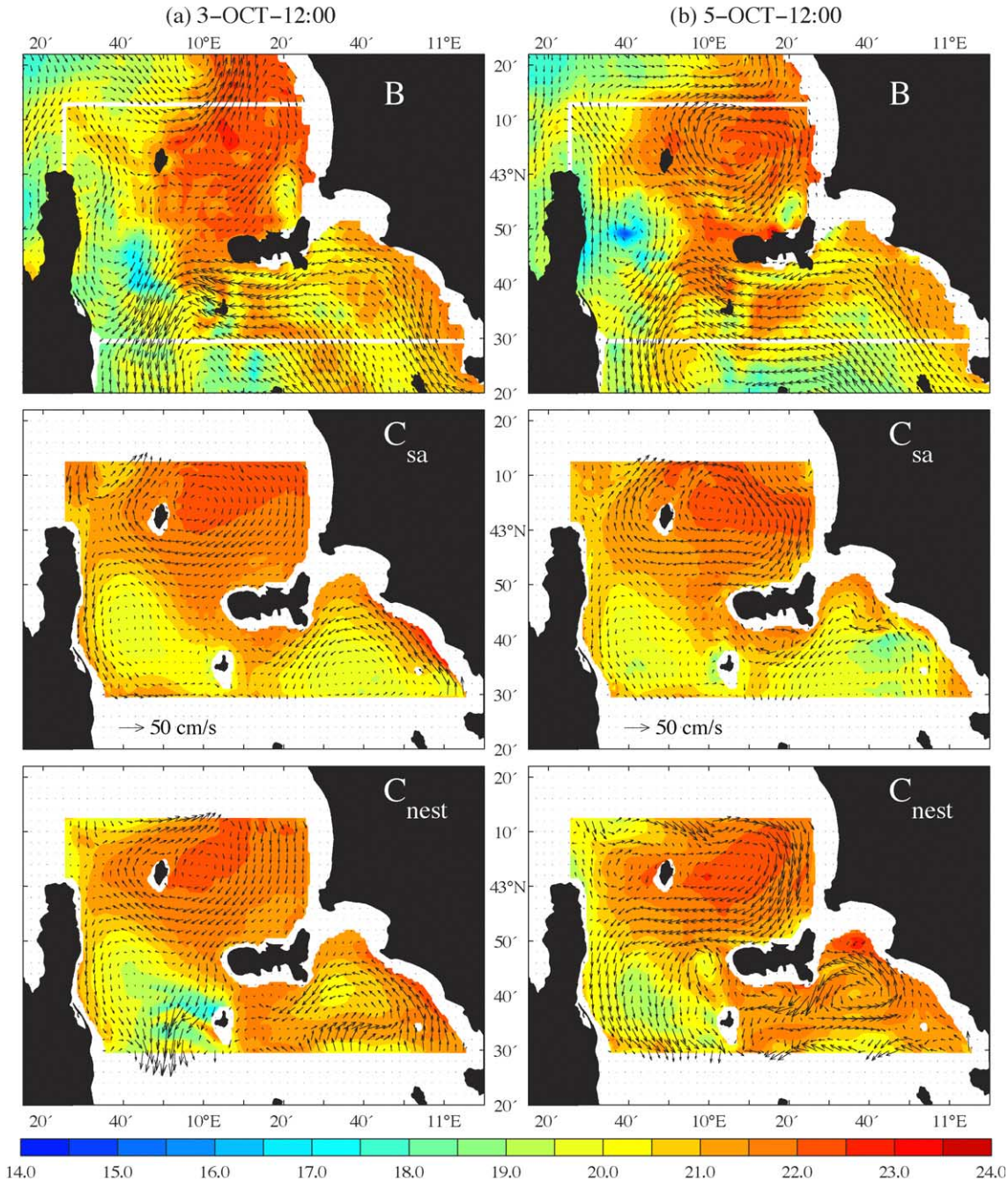

Fig. 6. Snapshots of 30-m velocity and temperature of model runs B (top), C_{sa} (center), and C_{nest} (bottom) (a) at the beginning and (b) towards the end of the nested configuration. The velocity scale is the same for all panels and indicated in the center panel.

The general distribution of the B domain SST is warm in the west (SST>22.8 °C) along Corsica and colder in the east with minimum temperatures of 20.6–21.8 °C between Elba and the mainland. The zonal width of the warm patch varies between 10 km at about the Elba latitude and 40 km at the latitude of Capraia and south of Pianosa island. This is reflecting the bands of westward flow north and south of Elba advecting cold water from the east. At 30-m depth, the large-scale situation is just opposite—higher temperatures above 22 °C are confined to the region between Elba, Capraia and the Italian mainland, while towards Corsica the temperature is generally below 20 °C. Here, even minimum temperatures below 15 °C are found at about 42°50′N on October 5.

5.2. The standalone C_{sa} domain

5.2.1. Horizontal velocity

The corresponding results of the C_{sa} model run are displayed in the second row of Figs. 5 and 6. The velocity patterns are similar to the B model results, but there are also significant differences. The northern Tyrrhenian cyclonic gyre is only partly reproduced in C_{sa}. While in the B domain it occupies almost the entire region south of Elba between Corsica and Italy, its zonal extent in C_{sa} is limited by Pianosa and Italy.

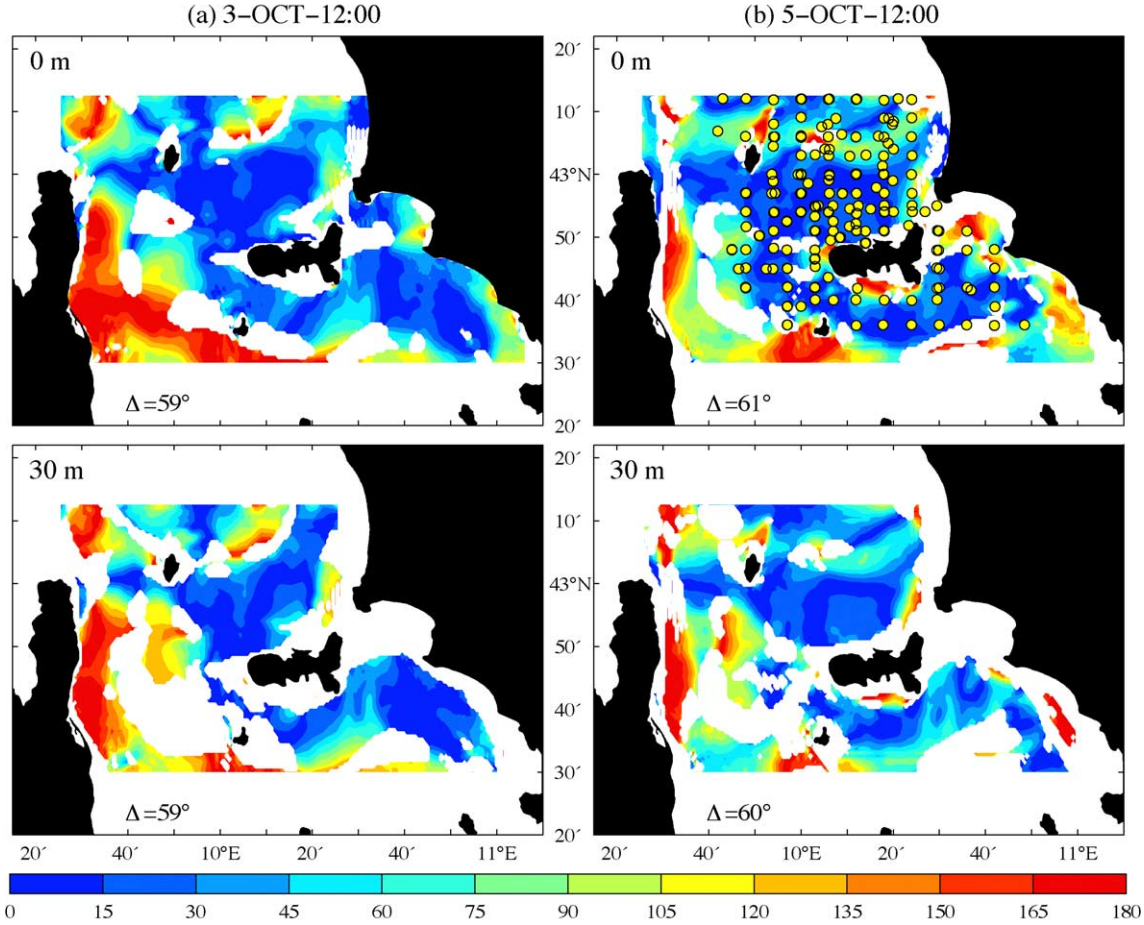

Fig. 7. Absolute difference of direction of horizontal velocity (°) between model runs C_{sa} and B at (a) the beginning and (b) towards the end of the nested configuration at the surface (top) and at 30-m depth (bottom). Areas where the speed in C_{sa} or B, respectively, is less than 5 cm s^{-1}, are left white. Yellow dots in (b) indicate the positions of casts during the update survey (cf. Fig. 2).

Namely, the flow pattern between Pianosa and Corsica is also cyclonic during most of the time, but a strong recirculation towards the Tyrrhenian off Corsica as in B is missing. The circulation pattern north of Elba is anticyclonic as in the B model. The inflow from the north off the Italian coast and the predominantly westward band of flow between Capraia and Elba are present in both domains. The Capraia Eddy is reproduced in C_{sa} as well, but it is somewhat different in shape, position and strength. Significant differences show up between Capraia and Corsica. In C_{sa}, there is a strong and narrow northeastward jet off Capraia, while in B there is no jet and a sluggish northwestward flow instead.

To quantify the above statements, we have plotted the differences of direction and speed of the surface and 30-m velocity between the C_{sa} model and the B model in Figs. 7 and 8, respectively. Concerning direction on 3 October, the difference is less than 45° in large areas around Elba, while it is greater near the boundaries of the C domain and off Corsica. On 5 October, the situation is similar, but in addition, larger deviations are noticeable along the Italian coast south of the Piombino Channel. For reference, we have added the positions of the casts of the update survey in Fig. 7b—the area updated by observations is clearly correlated with the small-difference region. Hence, the assimilation of casts apparently does a good job both

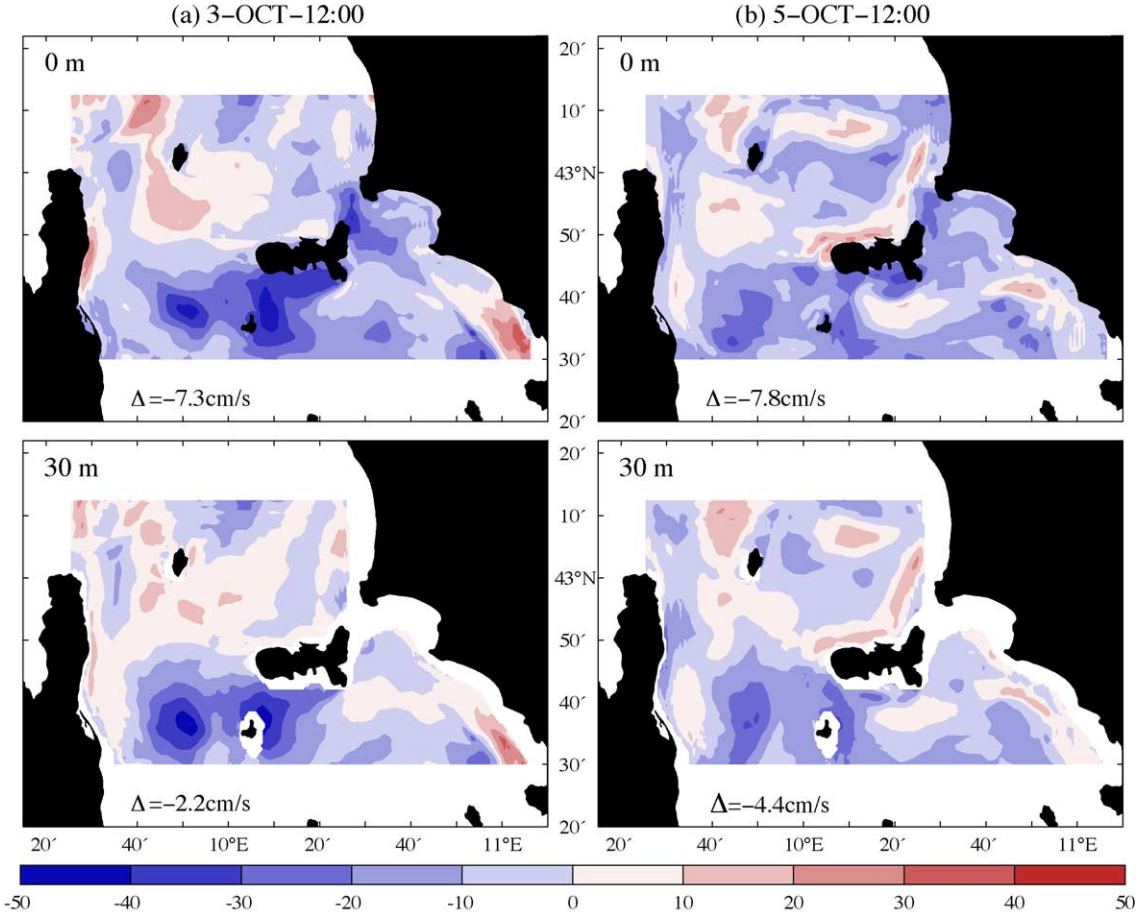

Fig. 8. Difference of speed (cm s^{-1}) between model runs C_{sa} and B at (a) the beginning and (b) towards the end of the nested configuration at the surface (top) and at 30-m depth (bottom). Red means that the speed in C_{sa} is greater than in B, while greater speed in B is indicated blue. Δ corresponds to the mean difference for each subplot.

in the B and the C_{sa} model. Concerning the differences of speed, there is no obvious correlation between the updated region and the magnitude of the difference (Fig. 8). In some regions, the speed is greater in C_{sa}, while in other areas it is the opposite, mainly south of Elba where the B model is more energetic. The latter results in the mean difference Δ being negative at all times. The reasons for this different behavior are many: it could be the different formulations of horizontal eddy diffusivity, different vertical mixing schemes, or simply differences between the applied atmospheric forcing fields, i.e. different resolution, drag coefficients or wind height. We will not discuss this in detail here, because it is beyond the scope of this investigation. However, attempts were made to compare the currents of both models with the observations displayed in Robinson et al. (submitted for publication), but such comparisons were not conclusive enough, because the direct observations were only from ship-borne ADCP, i.e. averaged over several days.

5.2.2. Temperature

Significant differences between C_{sa} and B are also noticeable in the surface temperature (Fig. 9, top panel). Absolute differences are generally less than

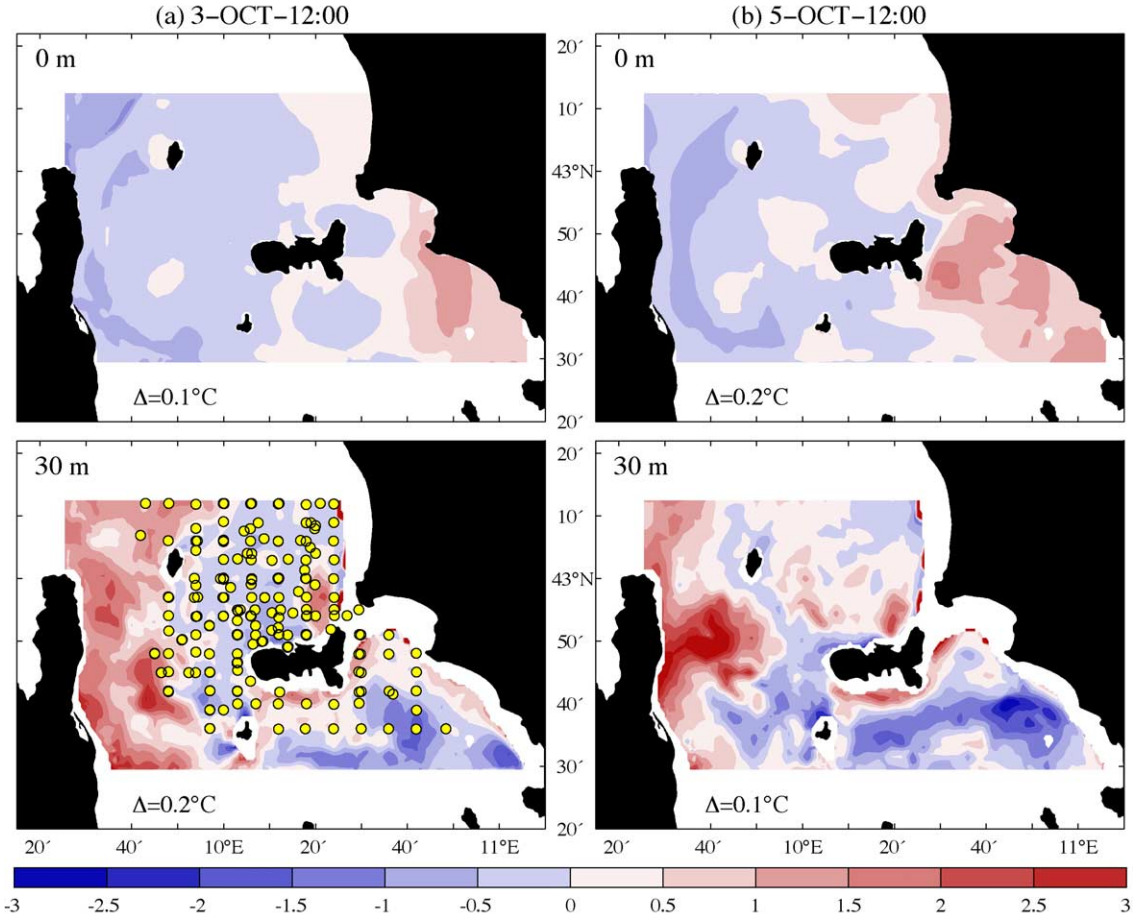

Fig. 9. Temperature difference (°C) between model runs C_{sa} and B at (a) the beginning and (b) towards the end of the nested configuration at the surface (top) and at 30-m depth (bottom). Red means that the temperature in C_{sa} is higher than in B, while higher temperature in B is indicated blue. Δ corresponds to the mean difference for each subplot. Yellow dots in (b) indicate the positions of casts during the update survey (cf. Fig. 2).

0.5 °C; higher values exceeding 1 °C are found between Elba and the Italian coast, where the C model is warmer, and off Corsica, where the C model is colder than the B model. On average, the C model is slightly warmer than the B model (Δ=0.1 °C on 3 October and Δ=0.2 °C 2 days later). A potential problem is the high temperature in the C domain along the Italian coast south of the Piombino Channel. As there is no indication for such high temperatures from the observations, it is concluded that it is due to false advection from the southern boundary. At first glance, this appears to contradict the statement above that the assimilation did a good job, but Fig. 2 reveals that all update casts in that region are either from September 28 and 29 or later than October 5. The C model was initialized on October 2, taking only account of the September casts; hence the observations east of Elba were not yet available for assimilation. By contrast, the latest SST from satellite was assimilated into the B model on 3 October, adjusting SST to the lower, probably correct value. One might conjecture that false advection also leads to higher temperature in C_{sa} along the northern boundary, but this is not true—according to Fig. 2, the latest update casts in this region were taken on October 3, thus the temperature rise is supported by observations.

At 30-m depth, the amplitude of the temperature difference is much larger (lower panel of Fig. 9). Although the average difference of 0.2 and 0.1 °C is comparable to that in the surface layer indicating once more the C_{sa} domain being warmer than B, large positive differences exceeding 2.5 °C are found in the region close to Corsica not covered by the update surveys. Further warm patches are found in the shallow waters south of Elba and between Elba and Capraia. It is conjectured that these differences are not due to lateral advection from the model boundaries, because the direction of the major streams is pointing out of the domains, at least those off Corsica, cf. Fig. 6. Instead, they are caused by slightly different values of the mixed layer depths among the models. These values are crucial, because the 30-m depth lies just below the base of the mixed layer in the upper thermocline. By contrast, the negative anomalies (B warmer than C_{sa}) south and southeast of Elba appear to be correlated with advection of warm water from southeast in the B domain.

5.3. C_{nest}: the impact of nesting via boundary assimilation

The results described above have revealed that within the C domain there are differences between the solutions of the B and the C_{sa} model. Hence, it is expected that the patterns in the C domain change when imposing the B domain solution along its boundaries.

5.3.1. Direction of horizontal velocity

The directional difference between C_{nest} and C_{sa} displayed in Fig. 10 exhibits rather similar structures at the surface and at 30-m depth. On 3 October, differences exceeding 45° are confined to the southern boundary, the region southwest of Elba, the Piombino Channel, and some patches along the northern boundary. The large values in the south are not surprising, because of the rather different velocity structure in the B and the C_{sa} domain, seen in Figs. 5 and 6 on the corresponding day. From the same figures, it becomes evident that C_{nest} has "learned" from B: instead of a weak eastward flow between Corsica and Pianosa in C_{sa}, C_{nest} has adapted to the strong southward current. In the same way farther east, along the southern boundary between Pianosa and about 10° E 50′, C_{nest} feels the stronger northward inflow dictated by B. The patch at the northern boundary close to the Italian mainland is aligned with the eastern flank of the Capraia anticyclone, the flow of which has a more southerly direction in B compared to C_{sa}. Although the C_{nest} flow pattern close to the open boundaries frequently has veered to the direction prescribed by B, there are also regions where the boundary assimilation seemed to fail, e.g. in the northwest corner of the C domain and north of Capraia. Here, the direction of flow in B is to the northwest and east, respectively, while it is southward and northeastward in C_{sa}. Surprisingly, the C_{nest} flow pattern is more aligned with C_{sa} instead of B. As we are convinced that our boundary assimilation scheme was technically correct, the only explanation for this behavior is that the total B flow here is largely barotropic or divergent (note that only the rotational part of the internal mode velocity was assimilated), and therefore the assimilated fraction was not felt by C_{nest}.

Two days later on 5 October, the mean directional difference has increased to 49° at the surface and 46°

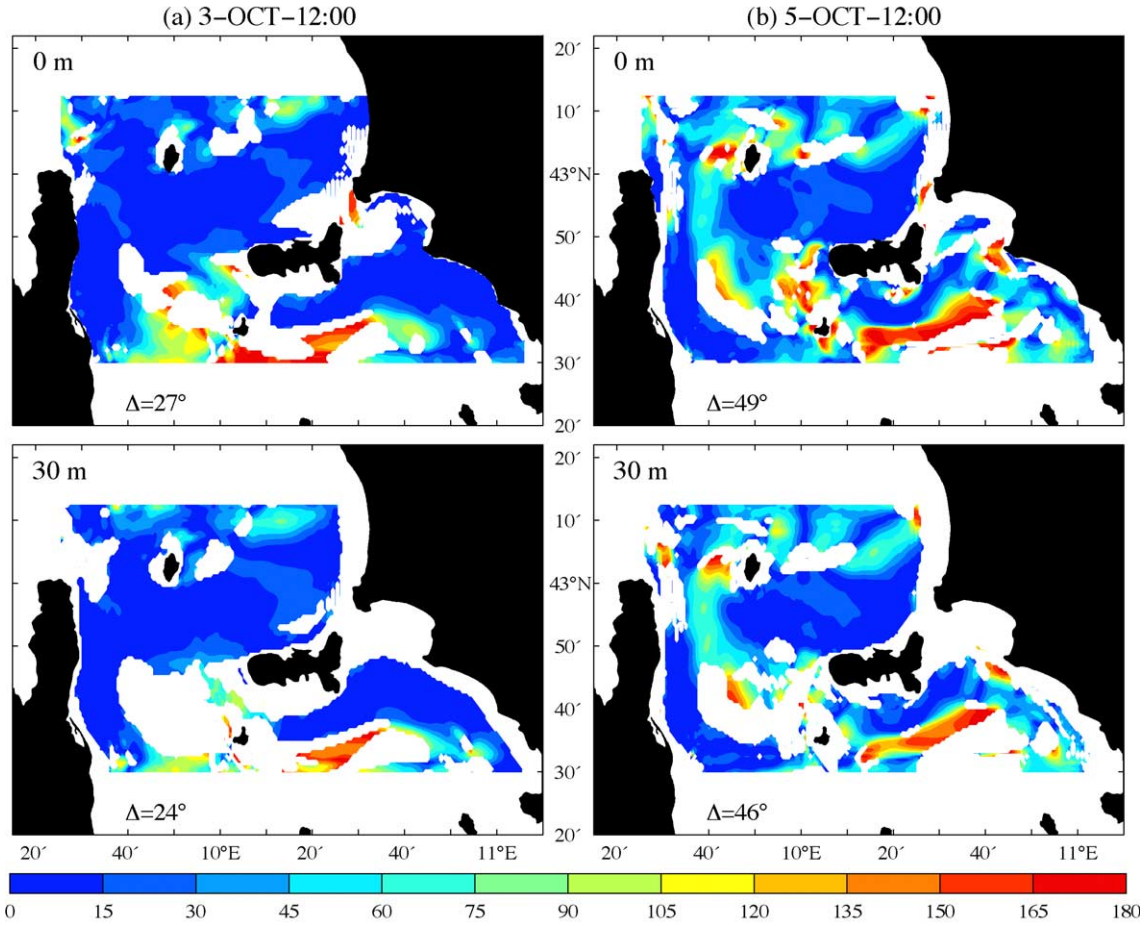

Fig. 10. Absolute difference of direction of horizontal velocity (°) between model runs C_{nest} and C_{sa} at (a) the beginning and (b) towards the end of the nested configuration at the surface (top) and at 30-m depth (bottom). Areas where the speed in C_{nest} or C_{sa}, respectively, is less than 5 cm s^{-1}, are left white.

at 30-m depth, while the corresponding values for 3 October have been 27° and 24°, respectively. In contrast to the situation 2 days earlier, the largest values are no longer attached to the open boundaries, but they have moved into the interior of the C domain. This is supported by the fact that near the boundaries the B model flow pattern on 5 October resembles more that of the C_{sa} model than on 3 October (cf. also Fig. 7). Apparently, the continuous assimilation of observed data from the update surveys impacted the solution of both domains in a way that they became more similar. However, in the interior the similarity between C_{sa} and C_{nest} decreased, e.g. at the Capraia latitude, in a meridional stripe parallel to the Corsica coast, and west and south of Elba.

5.3.2. Horizontal speed

Fig. 11 shows the impact of nesting on the speed in the C domain. On 3 October both at the surface and 30-m depth, major differences between C_{nest} and C_{sa} are confined to the southern open boundary and to a small area north of Capraia. Only here, the absolute values exceed 10 cm s^{-1}, reaching extreme amplitudes of more than 50 cm s^{-1} between Pianosa and Corsica and close to −40 cm s^{-1} in the southeast corner. The previous finding that the B model is more energetic than C_{sa} is reflected by the fact that near the open boundaries the differences are positive, i.e. the nesting is pumping energy into the C domain. The Δ values of 0.9 and 1.3 cm s^{-1} point in the same direction.

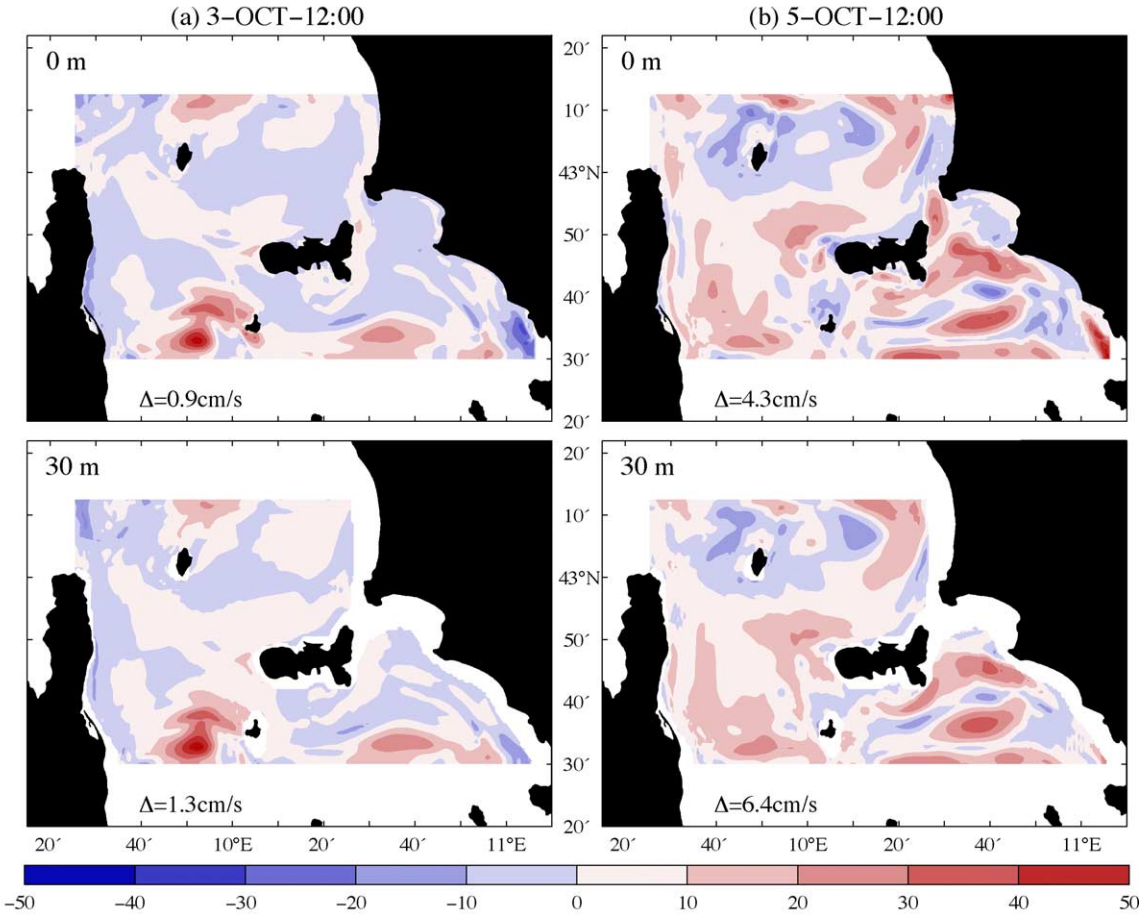

Fig. 11. Difference of speed (cm s^{-1}) between model runs C_{nest} and C_{sa} at (a) the beginning and (b) towards the end of the nested configuration at the surface (top) and at 30-m depth (bottom). Red means that the speed in C_{nest} is greater than in C_{sa}, while greater speed in C_{sa} is indicated blue. Δ corresponds to the mean difference for each subplot.

Three days later on 5 October, Δ has increased to 4.3 cm s^{-1} at the surface and 6.4 cm s^{-1} at 30-m depth; the values are again positive, hence the overall growth of kinetic energy has continued. But now, the increase is not confined just to the open boundaries, but has occurred also in the interior of the C domain.

5.3.3. Temperature

Both at the surface and at 30-m depth, the magnitude of the mean temperature difference Δ between C_{nest} and C_{sa} is increasing with time, which means that the boundary assimilation does the right thing (Fig. 12).

At the surface on 3 October, C_{sa} is becoming significantly (i.e. >0.5 °C) warmer than C_{sa} in the northwest corner and significantly colder in the southeast corner, only. In both cases, these differences would be consistent both with B domain temperature assimilation or cross-boundary advection, which is directed into the C domain (cf. Fig. 5).

On 5 October, the cool patch in the southeast has increased, now reaching north to about the Elba latitude. Apparently, the cooling is driven by the strong northwestward B domain flow across the C domain southern boundary. This is well expressed in Fig. 5a (bottom) but appears to become weaker with progressing time (Fig. 5b). The latter figure also shows that the strong inflow from the southeast has generated an anticyclonic vortex between Elba and the Italian mainland, advecting warm surface water

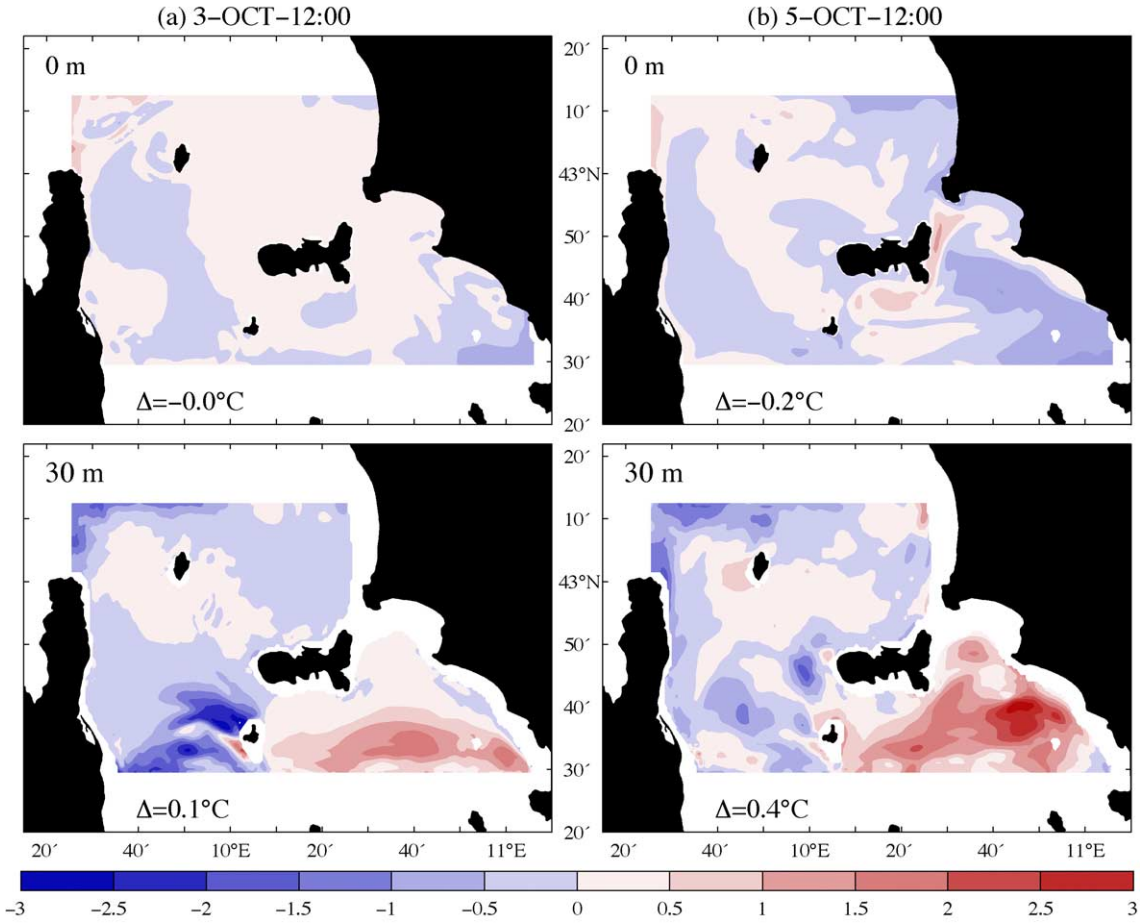

Fig. 12. Temperature difference (°C) between model runs C_{nest} and C_{sa} at (a) the beginning and (b) towards the end of the nested configuration at the surface (top) and at 30-m depth (bottom). Red means that the temperature in C_{nest} is higher than in C_{sa}, while higher temperature in C_{sa} is indicated blue. Δ corresponds to the mean difference for each subplot.

to the East Coast and south of Elba. This heating by more than 1 °C is visible in Fig. 12b as well. A second cooling region driven by the southward flow of the Caparaia anticyclone shows up between Capraia and the Italian mainland. The anticyclonic flow is more pronounced in the B domain being colder, and reducing the C domain temperature accordingly.

More dramatic changes of temperature occur at 30-m depth (bottom panels of Fig. 12). On 3 October, intense cooling of more than 2 °C amplitude is noticed between Pianosa and Corsica. This can neither be explained in terms of local assimilation of temperature nor in terms of horizontal advection. In fact, it is vertical motion exceeding 0.5 cm s^{-1} (Fig. 13) and driven by the strong southward horizontal advection in that area. This southward flow was not present in the C_{sa} domain (center panel of Fig. 5a), and the boundary assimilation of B domain horizontal velocity (bottom panel of Fig. 5a) has imposed divergent flow in the near surface layers, sucking cold water from below. By contrast, it has been verified that the warming southeast of Elba is not caused by vertical motion, but by boundary assimilation of temperature and horizontal velocity.

Two days later, the pattern of temperature difference is similar to that on 3 October. The warming region southeast of Elba has increased in size, and the

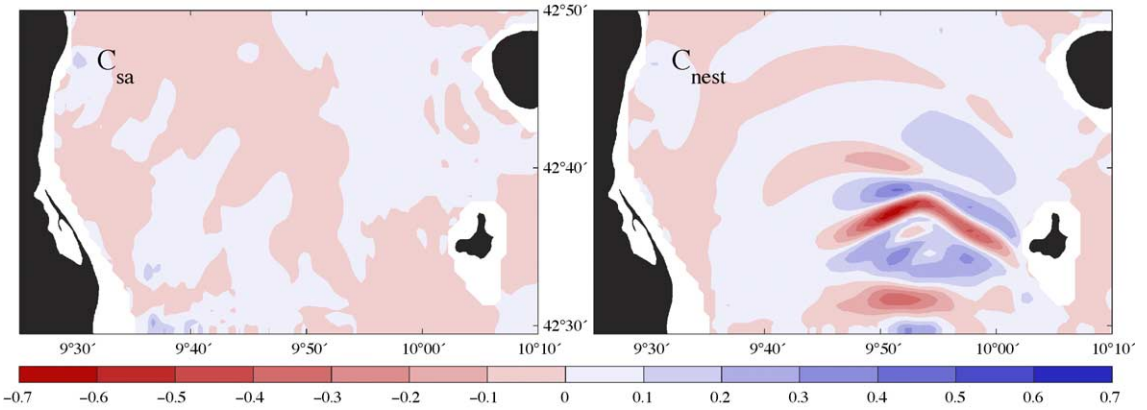

Fig. 13. Vertical motion (in cm s^{-1}) at 30-m depth between Corsica and the island of Pianosa in models C_{sa} and C_{nest}. Upwelling is indicated blue, downwelling red.

amplitude now reaches more than 2 °C. Maximum warming is found close to the Italian mainland, which appears to be a consequence of the combined effects of advection from the south and the water masses becoming stagnant due to the generation of the anticyclonic vortex mentioned above. The cooling between Pianosa and Corsica is still visible, but the amplitude has decreased. More intense cooling than 2 days before is noticed in the northwest corner, while a warming region did evolve at the northern boundary close to the Italian mainland. This is certainly an effect of the southward advection of the Capraia anticyclone, the eastern recirculation of which is stronger than 2 days earlier in the B domain (cf. top panel of Fig. 6b).

6. Summary and conclusions

In fall 2000, a heterogeneous team of ocean modelers from four different institutions was faced with the problem of setting up a chain of nested ocean circulation models ranging from basin to local scale. While the final local model was intended to zoom into the waters around the island of Elba at a horizontal resolution of the order of 100 m, the only available model at that time was a basin scale Mediterranean model at 10-km resolution. In order to bridge the gap of two orders of magnitude in resolution and domain size, a mesoscale and a sub-mesoscale model were additionally implemented. The final set of models consisted of four domains at 10 km, 3 1/3 km, 675 m and 225 m resolution, being nested into each other and referred to as the A, B, C and D domains.

The actual task was to issue daily forecasts of the oceanic environment for the C and D domains, hence special effort was required to get the dynamics right at these scales, depending largely on the formulation of the open boundary conditions for each of these domains. At the local scale this was not a problem, because the Harvard Ocean Prediction System (HOPS) was utilized for the C and D domains, and well-tested existent two-way nesting algorithms were applied (cf. Onken et al., 2003). The big challenge, however, was the derivation of open boundary conditions for the C domain. This was not trivial, because the superdomain encompassing the C domain was not HOPS, but CUPOM. CUPOM is different from HOPS in terms of horizontal and vertical coordinates and bathymetry, hence conventional nesting techniques could not be utilized.

A first attempt was made to construct a traditional one-way nesting between the B and C domains, i.e. to update the C domain open boundaries at regular intervals by interpolation of the B domain prognostic fields. This attempt failed, mainly because no mass conserving algorithm was found due to the non-alignment of the bathymetry and the land mask in CUPOM and HOPS. In order to overcome these problems, we developed a nesting method named *boundary assimilation*. Instead of prescribing the prognostic variables of the superdomain only at the open boundaries, they were assimilated in the entire

region of the nest, the assimilation weight being maximal at the boundary and then decreasing rapidly to zero towards the interior of the nest. The latter was done to enable a smooth transition between the domains and to allow the nested domain to develop its own dynamical characteristics.

There are numerous advantages to this new method in comparison with traditional one-way nesting:

- For assimilation in the nested domain, data of the superdomain are treated in the same way as observational data, i.e. as one-dimensional profiles. Hence, existing data assimilation procedures (e.g. Optimum Interpolation) can be utilized.
- There are no restrictions with respect to the horizontal or vertical arrangement of grid points, bathymetry or landmask in the superdomain.
- No special efforts are required concerning conservation of mass, as long as the horizontal velocity fields to be assimilated are non-divergent.
- Boundary assimilation guarantees a smooth transition between the domains. This is important, if the fields in the superdomain are very much different from the nest.
- Provision of superdomain profiles is easy—it is only necessary to extract profiles from the overlapping region.
- Boundary assimilation schemes can be set up rather quickly, which is important for rapid assessment of the oceanic environment in emergency situations, e.g. oil spills and search and rescue operations.

The new method has been extensively tested in terms of nesting the C domain into the B domain. We have run the C domain both in nested and unnested standalone mode, and assessed the impact of boundary assimilation by comparing the prognostic fields of the nested C domain with those in the standalone domain. Comparisons were carried out for the near surface fields and at 30-m depth. We found that the tracer and velocity fields responded rapidly to the boundary assimilation. Already at the instant when the first cycle was assimilated, the C domain fields exhibited clear signature of the B domain patterns mainly in the vicinity of the open boundaries. With progressing time and continued boundary assimilation, the differences between the nested and the standalone C domain were increasing, affecting also the interior of the C domain. This may be an undesired effect, which can be reduced by limitation of the width of the stripe where data are assimilated, or selection of smaller weighting coefficients. This is the price to be paid for nesting. Alternatively, the nest has to be run in standalone mode only, taking the risk of instabilities and false advection for longer-term integrations. Although it is beyond the scope of the present investigations, it would have been interesting to quantify the impact of boundary assimilation on the C domain structures in terms of a forecast skill evaluation. However, this would require a quasi-synoptic validation data set towards the end of the forecast period which is not available. Unfortunately on October 5, there were only seven casts which is definitely insufficient for skill evaluation. One day earlier on October 4, there were 22 casts, but this instant is too close to the HOPS initialization time. Moreover, all potential casts for skill evaluation are confined to a rather small region north of Elba which in addition would make a skill evaluation meaningless. Unfortunately, there were no more casts available, because this was not an experiment focusing only on ocean circulation.

The modeling effort described above has been carried out within the scope of Rapid Environmental Assessment (REA), requiring daily updates of ocean forecasts and a turn-around time of a day or less from the instant when the measurements are taken until the forecast is released. We have shown that this is feasible using modern Internet communication technology, even when the project partners are distributed all around the globe.

Acknowledgments

This study is based on oceanographic data, collected by the NRV *Alliance* under the scientific leadership of Francesco Spina and Alberto Alvarez. We appreciate the skill and the motivation of the masters and the crews, and the work done by the technical staff of the SACLANT Undersea Research Centre. We are grateful to Alex Trangeled and Ferry Vinck who designed the MEANS data flow and kept it running smoothly during the entire experiment. This study was supported by the Office of Naval Research

under grant N00014-97-1-0239 to Harvard University, and grant N00014-99-1-0788 to the University of Colorado. We thank NAVOCEANO for providing operational SWAFS fields for the Mediterranean Sea in real time for use in this project. SC acknowledges the support received by the European project MAS3 CT97 OT45 "F -ECTS".

References

Artale, V., Astraldi, M., Buffoni, G., Gasparini, G.P., 1994. Seasonal variability of the gyre-scale circulation in the northern Tyrrhenian Sea. J. Geophys. Res. 99 (C7), 14127–14137.

Astraldi, M., Gasparini, G.P., 1994. The seasonal characteristics of the circulation in the Tyrrhenian Sea. In: La Violette, P.E. (Ed.), The Seasonal and Interannual Variability of the Western Mediterranean Sea. Coastal and Estuarine Studies, vol. 46. American Geophysical Union, Washington D.C., pp. 115–134.

Bang, I.K., Chai, J.K., Kantha, L.H., Horton, C., Clifford, M., Suk, M.S., Chang, K.I., Nam, S.Y., Lie, H.J., 1996. A hindcast experiment in the East Sea (Sea of Japan). La Mer 34, 108–130.

Blumberg, A., Mellor, G., 1987. A description of a three-dimensional ocean circulation model. In: Heaps, N.S. (Ed.), Three-Dimensional Coastal Circulation Models, Coastal and Estuarine Science, vol. 4. American Geophysical Union, Washington D.C., pp. 1–16.

Carniel, S., Kantha, L.H., Franchi, P., Bergamasco, A., Umgiesser, G., 2001. A real-time nowcast/forecast experiment in the Ligurian Sea during GOATS/MEANS 2000: preliminary results, CNR-ISDGM Technical Report, 243, Venice (Italy), 44 pp.

Carniel, S., Umgiesser, G., Kantha, L.H., Monti, S., Sclavo, M., 2002. Tracking the drift of a human body in a coastal ocean using numerical prediction models of the oceanic, atmospheric and wave conditions. Sci. Justice 42, 143–151.

Carter, E.F., Robinson, A.R., 1987. Analysis models for the estimation of oceanic fields. J. Atmos. Ocean. Technol. 4, 49–74.

Horton, C., Clifford, M., Schmitz, J., Kantha, L.H., 1997. A real-time oceanographic nowcast/forecast system for the Mediterranean Sea. J. Geophys. Res. 102 (C11), 25123–25156.

Kantha, L.H., Clayson, C.A., 1994. An improved mixed layer model for geophysical applications. J. Geophys. Res. 99 (C12), 25235–25266.

Kantha, L., Chai, J.K., Leben, R., Cooper, C., Vogel, M., Feeney, J., 1999. Hindcasts and real-time nowcast/forecasts of currents in the Gulf of Mexico. Offshore Technology Conference (OTC '99) May 3–6, Houston, TX.

Kantha, L.H., Carniel, S., Franchi, P., 2002. Development of a real-time nowcast/forecast system for the Ligurian Sea: the GOATS-MEANS 2000 experiment. In: Bovio, E., Schmidt, H. (Eds.), The GOATS Joint Research Project: Underwater Vehicle Networks for Acoustic and Oceanographic Measurements in The Littoral Ocean, SACLANT Undersea Research Centre. La Spezia (Italy), pp. 275–288.

Krivosheya, V.G., 1983. Water circulation and structure in the Tyrrhenian Sea. Oceanology 23 (2), 166–171.

Krivosheya, V.G., Ovchinnikov, I.M., 1973. Peculiarities in the geostrophic circulation of the waters of the Tyrrhenian Sea. Oceanology 13, 822–827.

Lermusiaux, P.F.J., 1997. Error subspace data assimilation methods for ocean field estimation: theory, validation and applications. Harvard Open Ocean Model Reports, vol. 55. Harvard University, Cambridge, MA. 402 pp.

Lopez, J.W., Kantha, L.H., 2000. A data-assimilation numerical model of the North Indian Ocean. J. Atmos. Ocean. Technol. 17, 1525–1540.

Lozano, C.J., Robinson, A.R., Arango, H.G., Gangopadhyay, A., Sloan, Q., Haley Jr., P.J., Anderson, L.A., Leslie, W.G., 1996. An interdisciplinary ocean prediction system: assimilation strategies and structured data models. In: Malanotte-Rizzoli, P. (Ed.), Modern Approaches to Data Assimilation in Ocean Modeling, Elsevier Oceanography Series, vol. 61. Elsevier, Amsterdam, pp. 413–452.

Mellor, G.L., Yamada, T., 1982. Development of a turbulence closure model for geophysical fluid problems. Rev. Geophys. Space Phys. 20, 851–875.

Niiler, P.P., Kraus, E.B., 1977. One-dimensional models of the upper ocean. In: Kraus, E.B. (Ed.), Modeling and Prediction of the Upper Layers of the Ocean. Pergamon Press, Oxford, pp. 143–172.

Onken, R., Robinson, A.R., Haley Jr., P.J., Lermusiaux, P.F.J., Anderson, L.A., 2003. Data-driven simulations of synoptic circulation and transports in the Tunisia–Sardinia–Sicily region. J. Geophys. Res. 108 (C9), 8123.

Orlanski, I., 1976. A simple boundary condition for unbounded hyperbolic flows. J. Comp. Physiol. 21, 251–269.

Pacanowski, R.C., Philander, S.G.H., 1981. Parameterization of vertical mixing in numerical models of tropical oceans. J. Phys. Oceanogr. 11 (11), 1443–1451.

Robinson, A.R., 1996. Physical processes, field estimation and an approach to interdisciplinary ocean modeling. Earth-Sci. Rev. 40, 3–54.

Robinson, A.R., 1999. Forecasting and simulating coastal ocean processes and variabilities with the Harvard Ocean Prediction System. In: Mooers, C.N.K. (Ed.), Coastal Ocean Prediction, Coastal and Estuarine Studies Series. American Geophysical Union, Washington D.C., pp. 77–100.

Robinson, A.R., Walstad, L.J., 1987. The Harvard open ocean model: calibration and application to dynamical process forecasting and data assimilation studies. J. Appl. Numer. Math. 3, 89–121.

Robinson, A.R., Arango, H.G., Warn-Varnas, A., Leslie, W.G., Miller, A.J., Haley Jr., P.J., Lozano, C.J., 1996. Real-time regional forecasting. In: Malanotte-Rizzoli, P. (Ed.), Modern Approaches to Data Assimilation in Ocean Modeling, Elsevier Oceanography Series, vol. 61. Elsevier, Amsterdam, pp. 377–410.

Robinson, A.R., Lermusiaux, P.J.F., Sloan, N.Q., 1998. Data assimilation. In: Brink, K.H., Robinson, A.R. (Eds.), The Sea, vol. 10. John Wiley & Sons, New York, pp. 541–594.

Robinson, A.R., Sellschopp, J., Leslie, W.G., Onken, R., Alvarez, A., Baldasserini, G., Haley Jr., P.J., Lermusiaux, P.F.J., Lozano, C., Nacini, E., Stoner, R., Zanasca, P., 2004. Forecasting synoptic transients in the eastern Ligurian Sea. J. Mar. Syst. (submitted for publication).

Shapiro, R., 1970. Smoothing, filtering, and boundary effects. Rev. Geophys. Space Phys. 8, 359–387.

Spall, M.A., Robinson, A.R., 1990. Regional primitive equation studies of the Gulf Stream meander and ring formation region. J. Phys. Oceanogr. 20, 985–1016.